
Quantifying Information Leakage from Gradients

Fan Mo
Imperial College London

Anastasia Borovykh
Imperial College London

Mohammad Malekzadeh
Imperial College London

Hamed Haddadi
Imperial College London

Soteris Demetriou
Imperial College London

Abstract

Sharing deep neural networks' gradients instead of training data could facilitate data privacy in collaborative learning. In practice however, gradients can disclose both private latent attributes and original data. Mathematical metrics are needed to quantify both *original* and *latent* information leakages from gradients computed over the training data. In this work, we first use an adaptation of the empirical \mathcal{V} -information to present an information-theoretic justification for the attack success rates in a *layer-wise manner*. We then move towards a deeper understanding of gradient leakages and propose more general and efficient metrics, using *sensitivity* and *subspace distance* to quantify the gradient changes *w.r.t.* original and latent information, respectively. Our empirical results, on six datasets and four models, reveal that gradients of the first layers contain the highest amount of original information, while the classifier/fully-connected layers placed after the feature extractor contain the highest latent information. Further, we show how training hyperparameters such as gradient aggregation can decrease information leakages. Our characterization provides a new understanding on gradient-based information leakages using the gradients' sensitivity *w.r.t.* changes in private information, and portends possible defenses such as layer-based protection or strong aggregation.

1 Introduction

The training process of deep neural network (DNN) models is increasingly outsourced to the participants' devices, *a la* collaborative/federated learning [1, 2], due to distributed computational powers and data privacy issues. Instead of sharing private data, participants communicate the model/gradients updated on their data. However, as has been noted in recent work, the *shared gradients* can still leak private information which can be exploited by attacks such as input data reconstruction [3, 4] aiming to restore the original data, and attribute inference [5] aiming to infer latent attributes of the data.

Attacks on gradients are shown to be effective in practice [6–10], but more fundamentally, it is not clear when and to what degree different types of private information are stored in the gradients. Existing research considers information leakage to be a result of insufficient generalization performance or unintended memorization [11–13], but the specifics are still seen as an open problem. To understand DNNs' behavior, previous research has proposed analyzing the information flow through the DNN model's *layers* using a broad range of approaches *e.g.*, Shannon mutual information (MI) [14–17] and intermediate representation visualization [18–20]. However, since these methods focus on the *forward propagation*, they can fail to explain information leakages in terms of gradients produced in the *backward propagation*. As we demonstrate in the next section, both MI and visualization (*i.e.*, t-SNE projection) give the wrong characterization on which layers' gradients have higher information leakages. Therefore, there is a need for tools to systematically investigate, understand and measure such gradient-based information leakages.

In this work, we establish methodologies for characterizing information leakages from gradients in a *layer-wise manner*. The leakages are investigated on two main types of information: i) *original information*, the observed data in clients’ training datasets, and ii) *latent information*, attributes or properties of the observed data, in this way covering most existing critical attacks on gradients. We first propose using \mathcal{V} -information as an information-theoretical measure to give insight into *to what degree* information leakage happens. Then we present two easy-to-compute metrics that capture gradient changes *w.r.t.* original and latent information, respectively, to better understand *how* information leaks, by adapting sensitivity analysis and a subspace distance measure. We extensively evaluate the proposed metrics on six benchmark (images and text) datasets and four popular DNNs.

Contribution: i) We directly characterize private information *flow* in the gradients produced in the backward propagation. While the first layers of a model contain the most original information, our characterization is the first to reveal that layers of the classifier in most standard networks (*i.e.*, convolutional neural networks) contain the highest latent information. ii) We show that these layer-wise information leakages are highly predictable using gradient change measures, providing new insights to understand such leakages from gradients and a fast and effective way to assess the leakage levels of the layers. iii) We analyze the effect of training hyperparameters. We show that the epoch does not significantly influence information leakages, while gradient aggregation (*e.g.*, 30~50 times of non-target information) could significantly reduce information leakages.¹

2 Notations and preliminaries

Notations. We use lower-case italic, *e.g.*, x , for deterministic scalars, lower-case bold italic, *e.g.*, \mathbf{x} , for deterministic vectors, and upper-case bold italic, *e.g.*, \mathbf{X} , for deterministic matrices. Also, roman-type upper-case, *e.g.*, X , and lower-case, *e.g.*, x , denote random variables (of any dimensions) and their instances, respectively. See Appendix A.1 for a full summary of used notations.

Gradients sharing. In collaborative/federated learning, multiple clients collaboratively train a model while keeping the training data at the client’s side [1, 21]. More specifically, the gradient updated at one client (denoted as \mathbf{G}), is computed by $\frac{\partial \ell(\mathbf{X}, \mathbf{y}; \boldsymbol{\theta})}{\partial \boldsymbol{\theta}}$, where \mathbf{X} and \mathbf{y} denote one batch of training data and corresponding labels, $\boldsymbol{\theta}$ refers to model parameters, and $\ell(\cdot)$ refers to the loss function. This \mathbf{G} is a set of all model layers’ gradients which in typical federated learning settings is the minimum that must be shared to another participant (*e.g.*, server), corresponding to FedSGD approach. In FedAvg [1], models are consecutively updated on more batches of local data, which can be several epochs of training, and then shared. We note that a common way is to share the updated model $\boldsymbol{\theta} + \mathbf{G}$, but this practically amounts to sharing \mathbf{G} since all participants know $\boldsymbol{\theta}$. Besides, the gradient sharing can be among clients and the central server in any direction depending on different cases [22, 3, 21].

Attacks on gradients. The main intention of sharing gradients is to learn a model without revealing clients’ private data. However, adversaries can attack shared gradients to disclose i) original information, *e.g.*, directly reconstructing the clients’ data, and ii) latent information, *e.g.*, inferring attributes of the data. The *data reconstruction attack* (DRA) [3, 4, 8] works by randomly initializing dummy data and feeding it into the model to get dummy gradients. Then, the dummy data gets close to the real private data if the dummy gradients are optimized to get close to the real gradients. DRAs can reach high accuracy (*e.g.*, to a pixel-wise level for images) as shown in experiments [3, 8]. However, it may fail when gradients have sufficient aggregation (*e.g.*, a large batch size) because the optimization becomes hard to solve when the gradients of multiple images are mixed together. The *attribute inference attack* (AIA) [5, 23, 6] works better in stronger gradient aggregation. AIAs focus on extracting latent information, *i.e.*, private attributes of the client’s data. One way of attacking is to collect multiple snapshots of the model and feed them with the attacker’s own data with/without a certain target attribute to obtain corresponding gradients of the data. The gradients and their attribute labels are used to train a binary classifier that can distinguish whether an obtained set of gradients was computed on clients’ data with a target attribute or without it. Note that the presence of a particular client’s data in the training dataset, *e.g.*, explored by *membership inference attacks* [6], may be regarded as one attribute of the input, because membership leakage risks can be correlated to the attribute leakage risks [11].

Layer-wise analysis. To investigate the root cause of the above-mentioned information leakages, the research on DRAs [3] computed the mean square error loss between dummy and real gradients

¹Codes are anonymously available through the following link: <https://bit.ly/3fn7nzz>

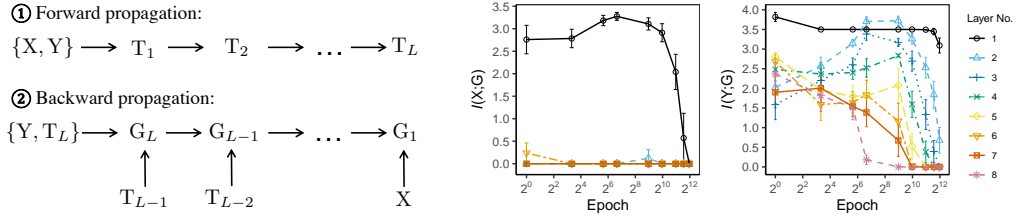


Figure 1: [Left] Markov chain in forward propagation (from layer 1st to L^{th}) and backward propagation (from layer L^{th} to 1st). G refers to gradients; T refers to intermediate representations. [Right] Mutual information between gradients and inputs/labels (*i.e.*, $I(X; G)$ and $I(Y; G)$, respectively).

layer-wisely, showing that the last layer has the smallest loss. However, this result is not suitable for comparison across layers since the calculation of losses depends on layer sizes which usually are different among layers. Besides, the smallest loss does not necessarily result in the highest attack performance, and thus, the loss cannot give the correct insight into the underlying cause of information leakage. The research on AIAs also included a layer-wise analysis [5] using t-SNE projection [24]. It performs a dimensionality reduction on layers’ outputs to visually explain why the inference attack can exploit unintended attribute information. Results show that these attributes are clustered in the former layers while the class label is clustered in the last layer. However, the analysis is on outputs (in the forward propagation) instead of gradients that the attack actually uses.

There exists a line of works analyzing the forward information flow or representations of inputs in a layer-wise manner [25–27]. Visualizations of intermediate representations (*i.e.*, layers’ outputs) and filters indicate that former layers focus on learning general information about inputs (*e.g.*, ambient colors in images), while latter layers learn specific information related to the classification task (*e.g.*, face identity) [18–20]. More specifically, a theoretically grounded method based on Shannon mutual information (MI or $I(\cdot; \cdot)$) has been adopted to quantify the forward information flow [16, 15, 17]. For an observed data sample X , with the label Y , the layer-by-layer computations (from 1 to L) form a Markov chain (see Figure 1 left-①). Following this, $I(X; T)$ and $I(Y; T)$ should *not* increase during the forward propagation. However, this fails to explain the gradients (G) in the backward propagation because its Markov chain is constructed on the products of forward propagation (*i.e.*, T) as shown in Figure 1 left-②). As an example, we compute $I(X; G)$ and $I(Y; G)$ using the state-of-art MI neural estimation [28]. The results on a 8-layer DNN [14] trained on MNIST [29] show that layer 1st’s gradients always have the highest MI on both X and Y (see right Figure 1). Latter layers have lower $I(Y; G)$ except for the first several epochs. But the result that the first layers have the most information of Y is in conflict with the observation that most (high-level) membership information leakages happen in the last layers [6, 30, 31]. Thus, we still need to find a theoretical framework to correctly characterize information leakages from gradients.

3 Layer-wise information leakage

Information leakage definitions. We aim to characterize two forms of leakage related to i) *original information* and ii) *latent information* of the local input data. Original information leakage refers to the disclosure of the local training data [32, 3], and latent information leakage refers to the disclosure of latent information (*e.g.*, attributes) of the training data [5, 6]. In particular, let X (or \mathbf{X} when considering it as a deterministic variable) denote one client’s private training data, and let P (or \mathbf{p}) denote one type of latent information of the data. Then, the original information leakage risk is measured by how much information about X an adversary can extract, and the latent information leakage risk is measured by how much information about P an adversary can extract from the gradients. Although P can be extracted from X , we consider them separately as the cause and localization of the two types of information leakage are very different, and in real-life settings adversaries with certain requirements and model capacities aim at disclosing a certain kind of information.

3.1 Quantifying leakage by \mathcal{V} -information

Given that Shannon MI cannot properly explain information leakage from gradients, we adopt a variational extension of Shannon information theory known as \mathcal{V} -information [33]. It takes computational constraints into consideration (see Appendix A.3 for details) and informally is said to measure the ‘usable’ information. For example, one reasonably expects the latter layers in a model to extract features that are useful for the target task, so that usable information for the task Y memorized in model/gradients is increasing throughout the layers. Interestingly, the computation of empirical \mathcal{V} -information is highly similar to using the actual attack success rate. By defining the predictive family to be sufficiently general, computing it *once* will allow us to understand the success rate of all attacks that fit the family, thus providing theoretical guarantees based on obtained attack success rates. This gives a grounded way to measure the layer-wise information leakages by conducting attacks on each layer directly. In particular, the DRA indicates the information leakage risk of one layer’s gradients in terms of original data, while the AIA reflects the leakage risk of latent information.

More specifically, here we consider an adversary \mathcal{A} as a computationally bounded agent, who aims to predict the outcome of a real-valued random variable (*i.e.*, private original X or latent information P), based on side information *i.e.*, shared gradients. The adversary only has access to the attack models (denoted as $f_{\mathcal{A}}$) from the predictive family $\mathcal{V}_{\mathcal{A}}$ due to computational constraints or lack of adequate knowledge - we choose this family to be sufficiently general to encompass a wide amount of attackers. Because attacks and corresponding density measures of original and latent information are different, we define them separately as follows.

Latent information leakage risk. Let $G_l \in \mathbb{R}^{N_l \times N_{l-1}}$ be the layer l^{th} ’s gradients, where $N_l \times N_{l-1}$ denotes the dimensionality. Let p and g_l denote an instance of P and G_l , respectively. Let $f_{\mathcal{A}}[g_l] \in \mathcal{P}(\text{domain}(P))$ denote a probability measure on the domain of P chosen based on the side information g_l , where $f_{\mathcal{A}}[g_l](p) \in \mathbb{R}$ is the value of the density evaluated at some value of the random variable p . Similarly, $f_{\mathcal{A}}[\emptyset](p)$ is without the side information. We assume that the predictive family satisfies the optional ignorance condition (Definition 1 in Appendix A.3); something that, under certain assumptions, common attack models such as random forests (RF) [5] can satisfy. Let \mathcal{D} be the dataset that consists of all instances g_l, p . Let p_i denote the private information and $g_{l,i}$ denote the observed layer l^{th} ’s gradients for data sample i . The empirical \mathcal{V} -information from G_l to P evaluated on \mathcal{D} is:

$$\hat{I}_{\mathcal{V}_{\mathcal{A}}}(G_l \rightarrow P) = \inf_{f_{\mathcal{A}} \in \mathcal{V}_{\mathcal{A}}} \frac{1}{|\mathcal{D}|} \sum_{p_i \in \mathcal{D}} -\log f_{\mathcal{A}}[\emptyset](p_i) - \inf_{f_{\mathcal{A}} \in \mathcal{V}_{\mathcal{A}}} \frac{1}{|\mathcal{D}|} \sum_{g_{l,i}, p_i \in \mathcal{D}} -\log f_{\mathcal{A}}[g_{l,i}](p_i), \quad (1)$$

where the infimum over $\mathcal{V}_{\mathcal{A}}$ can be approximated using the best algorithm $f_{\mathcal{A}} \in \mathcal{V}_{\mathcal{A}}$ [33]. Note that we disregard \mathcal{D} in $\hat{I}_{\mathcal{V}_{\mathcal{A}}}(G_l \rightarrow P)$ for notational simplicity. Let $p_i \in \{0, 1\}$ denote the absence or presence of the latent attribute for sample i . Let v be the attackers’ model taking as input the gradient so that $v(g_{l,i})$ is the output. The predicted density value for p_i , *i.e.*, the softmax of v ’s output, is:

$$f_{\mathcal{A}}[g_{l,i}](p_i) = \frac{e^{\{v(g_{l,i})\}_{p_i}}}{e^{\{v(g_{l,i})\}_0} + e^{\{v(g_{l,i})\}_1}}, \quad (2)$$

and $f_{\mathcal{A}}[\emptyset](p_i) = \frac{1}{2}$, *i.e.*, the value of the uniform distribution over the outputs. Intuitively \mathcal{V} -information measures the difference in how likely a certain value of the property is to be observed under the density computed with and without gradient information, thus measuring how *valuable* gradient information is to the accuracy in inferring the property. When $f_{\mathcal{A}}[g_l]$ produces a perfect prediction with a loss equal to 0 on \mathcal{D} , the second item in Equation (1) is equal to 0 and consequently $\mathcal{V}_{\mathcal{A}}$ achieves the highest \mathcal{V} -information from G to P . In the worst case, $f_{\mathcal{A}}[g_l]$ produces a random prediction regardless of whether we use or not use side information g_l so the smallest \mathcal{V} -information is equal to 0. To achieve the infimum over $\mathcal{V}_{\mathcal{A}}$, we use the best RF in [5], with an attached softmax function during inference to evaluate the prediction results in probability density.

Original information leakage risk. Similarly to Equation (1), we can derive the empirical \mathcal{V} -information based on G_l for inferring X as $\hat{I}_{\mathcal{V}_{\mathcal{A}}}(G_l \rightarrow X)$. Let x denote an instance of X . In order to use \mathcal{V} -information, we require a density function over the input data. Here we construct an *approximation* of a density based on a combination of a Gaussian likelihood and a structural similarity index measure (SSIM) [34] used for measuring the perceived similarity between two high-dimensional inputs (*e.g.*, images). Regarding other types of data one can adopt measures in similar ways (*e.g.*, Peak Signal-to-Noise Ratio for audio). We remark once more that this is an approximation

of the density however as we will show numerically it is able to quantify the most at-risk layers correctly as judged by its correlation with the attack success rate. Our density approximation to be used in the original information variant of (1) is given by:

$$f_{\mathcal{A}}[g_{l,i}](x_i) = \frac{1}{\sqrt{2\pi}\sigma} e^{-\frac{(1-\text{SSIM}(v(g_{l,i}), x_i))^2}{2\sigma^2}}, \quad (3)$$

where $\text{SSIM}(v(g_{l,i}), x_i)$ measures the perceptual similarity between reconstructed and original data, such that $1 - \text{SSIM}$ gives the dissimilarity. SSIM can be computed as a combination of luminance (l), contrast (c), and structure (s):

$$\text{SSIM}(v(g_{l,i}), x_i) = l(v(g_{l,i}), x_i) \cdot c(v(g_{l,i}), x_i) \cdot s(v(g_{l,i}), x_i). \quad (4)$$

Functions of $l(\cdot)$, $c(\cdot)$, and $s(\cdot)$ are determined by the average and variance of both $v(g_{l,i})$ and x_i and their covariance (see [34] for details). SSIM is with a range of $[0, 1]$. This similarity is 0 for the worst prediction, and thus, $f_{\mathcal{A}}[\emptyset](x_i) = e^{-2\pi^2}$ for $\sigma = \frac{1}{2\pi}$. The best prediction gives $f_{\mathcal{A}}[g_{l,i}](x_i) = 1$. In addition, to achieve the infimum over $\mathcal{V}_{\mathcal{A}}$ for original information adversary, we choose the DNN-like model in [3] as the attack model.

3.2 Measuring changes in gradients

To further understand information leakages, it is desirable to make no explicit assumptions about the attackers' model; stronger attack methods proposed in future research may also not be covered in the chosen predictive family. We desire metrics computable using *solely* the gradients, which could simplify and make more efficient the computation of the measures. Understanding private information memorization by models, in particular in the updated gradients, can be related to the models' generalization ability: learning a model that generalizes well avoids the memorization of unnecessary information making its parameters insensitive to small changes in the inputs [35, 36, 11]. Based on this, if certain gradients are non-sensitive to changes in the input data or latent information, training a generator or classifier that would be highly successful in capturing the input or property changes will be challenging, which in turn makes the success rate of the attack low.

Sensitivity for original information. Sensitivity has been used in measuring model generalization [37, 38]. Sensitivity *w.r.t.* the *input* is a concept that quantifies to what extent the target variable (*i.e.*, *output*) is affected by small changes in the corresponding input variables. It has also been applied in measuring model robustness on adversarial example attacks [39, 40]. A model that is non-sensitive to certain changes in inputs is expected to have high robustness. On the other hand, by bounding the sensitivity of outputs *w.r.t.* inputs leveraging differential privacy, one can certify model robustness to changes in input *i.e.*, adversarial examples, proposed in [41].

Here we adapt sensitivity to quantify original information leakage from the gradients *i.e.*, sensitivity of the *gradient w.r.t.* the *input*. That is, if the gradient sensitivity is low and thus gradients change insignificantly when altering the input, reconstructing the input will be more challenging. More specifically, we can utilize the Jacobian matrix of the gradients *w.r.t.* the input (similar to input-output Jacobian [38, 37]) to reflect how sensitive the gradients are when changing the input, *i.e.*, a sensitivity measure on gradients. The input-gradient Jacobian is calculated by:

$$\mathbf{J}_l^{(G)}(\mathbf{X}) = \frac{\partial \mathbf{g}_l(\mathbf{X})}{\partial \mathbf{X}} = \frac{\partial}{\partial \mathbf{X}} \left(\frac{\partial \ell(\mathbf{X}, \mathbf{y}, \boldsymbol{\theta})}{\partial \boldsymbol{\theta}_l} \right), \quad (5)$$

where $\mathbf{g}_l(\cdot)$ represents the function that produces layer l^{th} 's gradients G_l . Besides, $\ell(\cdot)$ is the loss function over \mathbf{X} , ground truth \mathbf{y} , and parameters of the complete model $\boldsymbol{\theta}$, so $\mathbf{g}_l(\cdot)$ can be regarded as the partial derivative of $\ell(\cdot)$ *w.r.t.* layer l^{th} 's parameters $\boldsymbol{\theta}_l$ (*i.e.*, backward propagation).

Then we compute the Frobenius norm (referred to F -norm) of the above input-gradient Jacobian matrix similar to [38], which indicates the general input leakage risk. As in our case Jacobians are compared across layers with different sizes, we include two other norms, *i.e.*, 1-norm and the ∞ -norm. Using different norms will help in capturing adversaries with different capabilities, similar to the differential privacy in adversarial example [42, 41], where the p -norm reflects how the adversary measures distance between two data samples (*e.g.*, 1-norm considers all dimensions of the data sample, and ∞ -norm focuses on one dimension). Thus, given K data samples, we compute the Jacobian with p -norm (referred to as 'Jacobian p -norm' hereinafter) averaged over the data samples

as the leakage risk of the original information (\mathbf{X}) in layer l^{th} 's gradients:

$$\mathcal{R}_l^{(\mathbf{X})} = \mathbb{E}_{\Delta\mathbf{X}} \left[\|\mathbf{g}_l(\mathbf{X}) - \mathbf{g}_l(\mathbf{X} + \Delta\mathbf{X})\|_p \right] = \frac{1}{K} \sum_{k=1}^K \left\| \mathbf{J}_l^{(\mathbf{G})}(\mathbf{X}_k) \right\|_p \quad (6)$$

where $p = F, 1$, or ∞ . Note that the size of \mathbf{G}_l still has an impact on the computed sensitivity. A larger \mathbf{G}_l size can result in a larger sensitivity in terms of 1-norm and F -norm. When reconstructing high-dimensional input data, a large \mathbf{G}_l size is necessary, which can be reflected by these norms.

Subspace distances for latent information. For attacks on latent information, such as the attribute inference in [5], the success of the attack lies in the ability of the classifier to distinguish between whether certain gradients were computed over data that did or did not have a certain attribute. One may expect to compute the sensitivity of gradients *w.r.t.* latent information such as attributes. However, this is intractable because i) this latent information is not in the ML computational graph so to compute $\frac{\partial \mathbf{g}}{\partial \mathbf{p}}$ is not straightforward, and ii) a large number of inputs have the same latent information, and based on that, the attack's classifier only produces a binary prediction, while sensitivity (*e.g.*, in Equation (6)) measures each data point separately. Therefore, to quantify the changes in gradients, we follow a more direct way. First, we separate the target dataset into two parts based on the presence of one specific latent information, and then we compare the subspace distance between gradients computed on these two parts of the dataset. This still follows the same intuition as understanding how sensitive the gradients are *w.r.t.* latent information.

Without loss of generality, assume that dataset \mathcal{S} consists of two disjoint subsets \mathcal{S}_0 , whose samples do not have the target latent information, and \mathcal{S}_1 , whose samples have the target latent information. Then we obtain the corresponding gradients of layer l^{th} computed on these two subsets by:

$$\mathbf{G}_l^{(0)} = \mathbb{E}_{\mathbf{X} \in \mathcal{S}_0} [\mathbf{g}_l(\mathbf{X})] \text{ and } \mathbf{G}_l^{(1)} = \mathbb{E}_{\mathbf{X} \in \mathcal{S}_1} [\mathbf{g}_l(\mathbf{X})]. \quad (7)$$

For each pair of matrices $\mathbf{G}_l^{(0)}$ and $\mathbf{G}_l^{(1)}$ (in $l \in \{1, \dots, L\}$), let $\mathbb{G}_l^{(0)}$ and $\mathbb{G}_l^{(1)}$ denote their corresponding subspaces, respectively. To measure the difference between the computed gradients with and without target latent information, we can compute the Grassmann geodesic distance [43, 44] between these two subspaces as the leakage risk of this latent information \mathbf{p} in layer l^{th} 's gradients:

$$\mathcal{R}_l^{(\mathbf{p})} = \text{dist}(\mathbf{G}_l^{(0)}, \mathbf{G}_l^{(1)}) = d_{\text{Gr}(k,n)}(\mathbb{G}_l^{(0)}, \mathbb{G}_l^{(1)}) = \left(\sum_{i=1}^k \theta_i^2 \right)^{1/2}, \quad (8)$$

where $\text{Gr}(k, n)$ denotes the Grassmann manifold, and both $\mathbb{G}_l^{(0)}$ and $\mathbb{G}_l^{(1)}$ are elements of $\text{Gr}(k, n)$ and are k -dimensional linear subspace in \mathbb{R}^n . k is the layer l^{th} 's gradient size $N_l \times N_{l-1}$. θ_i for $i \in \{1, \dots, k\}$ are principal angles between the two subspaces which can be computed using numerical methods [45]. In this paper we use the Grassmann distance; other common distances defined on Grassmannians (*e.g.*, Asimov) [44] can be derived similarly.

4 Empirical results

Models and datasets. To evaluate our metrics, we use four models: LeNet, AlexNet, and VGG9-like [29, 46, 47] for image datasets, and a 4-layer model [48] (referred to as *TextClf*) for text datasets. TextClf is similar to the target models used for analyzing attacks in [5]. All models Conv layers are usually considered as the *feature extractor* capturing features of the input data, and FC layers are considered as the *classifier* performing classification on extracted features. We use four images datasets CIFAR-100 [49], Labeled Faces in the Wild (LFW) [50], Large-scale CelebFaces Attributes (CelebA) [51], and Public Figures Face Database (PubFig) [52], and two text datasets IMDB reviews [53] and CSI corpus [54] for model training and evaluation. See Appendix A.4 for details of the model architecture and used datasets.

4.1 Layer-wise information leakages

Original information by \mathcal{V} -information. We use the same setting (*i.e.*, model and hyperparameters) as DRAs in [3, 4] as the predictive family of \mathcal{V} -information. To measure layer-wise information leakage, we perform attacks on individual layers. As we found that existing DRAs are not successful

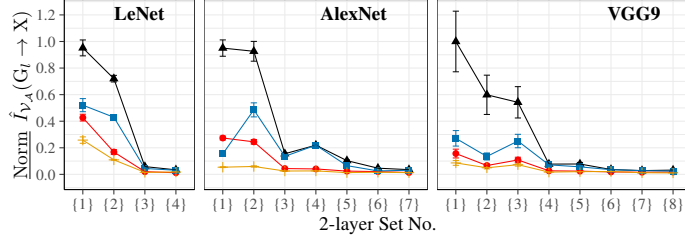


Figure 2: Original information leakage risks, measured by \mathcal{V} -information, in each 2-layer set’s gradients, based on CIFAR100 (—), LFW (—), CelebA (—), PubFig (—) datasets.

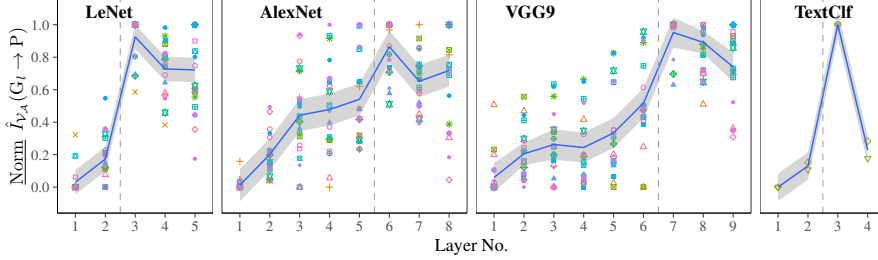


Figure 3: Latent information leakage risks, measured by \mathcal{V} -information, in each layer’s gradients. Scattered points refer to private attributes being measured for different datasets and classification tasks (see Appendix A.5). Blue lines give the LOESS regression curve. Dashed lines (- -) separate the feature extractor and the classifier of the model.

when using gradients of only one layer, we measure this leakage on the set of two consecutive layers at a time. Specifically, in Figure 2, set $\{1\}$ denotes layers 1st and 2nd, set $\{2\}$ denotes layers 2nd and 3rd, *etc.* Furthermore, we normalize the computed \mathcal{V} -information of one model with the maximum value of its layer for comparability across models and tasks. The results indicate that the original information leakage risk generally decreases when moving from the first 2-layer set to the last 2-layer set, although there exist slight fluctuations. This decreasing pattern agrees with the Markov chains in the Figure 1, where for both forward and backward propagation, G_1 and G_2 are closest to the X and T_1 ; thus encoding the most information original data. Besides, the information leakage risk for CIFAR100 is higher than for the other three face-image datasets. This could be due to the fact that in CIFAR100 images of different objects have richer features (*e.g.*, ambient colors and shapes) than face images, leading to more significant gradient changes that are easier to capture by attack models.

Latent information by \mathcal{V} -information. Here we use the same attack setting as in [5] for the predictive family for latent attribute inference. We additionally train the TextClf on the two text datasets and remove CIFAR100 because it does not have multiple attributes. Also, since each dataset can have multiple types of attributes considered as private latent information, we compute \mathcal{V} -information on all these attributes and then fit smooth curves using nonparametric local weighted (*i.e.*, LOESS) regression [55] to clarify the general trend across layers. As shown in Figure 3, the latent information leakage risk follows a trend that increases when moving through the feature extractor layers, reaches its maximum at the first classifier layer, and then decreases. This result is similar across all models. Compared to MI in Figure 1, the results from \mathcal{V} -information are more reasonable and in accordance with the attack results. The reason is that measuring with \mathcal{V} -information considers computational constraints of the attacker. More interestingly, the exact original information (*i.e.*, what is the exact input) mostly lies in the first layers as our analysis shows, and most existence/membership information (*i.e.*, whether this input exists in the training set or not) and classification task information (*i.e.*, labels) are in the last layers as found in previous research [6, 30, 31, 56], so it is expected that the latent information (*i.e.*, which attribute the input has) would be extracted from the middle layers.

4.2 Gradient changes indicating information leakages

Here we localize information leakages by measuring just the gradient changes, a method that is more general and easily-computable than \mathcal{V} -information but still well-able to capture the leakages.

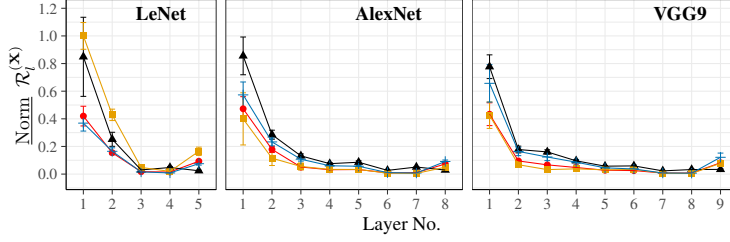


Figure 4: Original information leakage risks, measured by sensitivity, in each layer’s gradients, based on CIFAR100 (—), LFW (—), CelebA (—), PubFig (—) dataset.

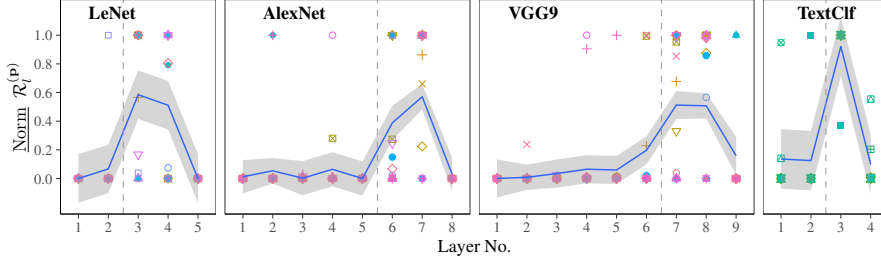


Figure 5: Latent information leakage risks, measured by subspace distances, in each layer’s gradients. Scattered points correspond to private attributes (see Appendix A.5).

Original information. We compute Equation (6) to measure original information leakage risks. Here we only show the measure of F -norm, as other p -norms give similar results (see Appendix A.6). As shown in Figure 4, overall the sensitivity shows a similar pattern as \mathcal{V} -information (in Figure 2). Specifically, gradients of the first layers are more sensitive to changes in inputs compared to latter layers, thus they could potentially carry more private original information that can be detected by adversaries easier. Besides, the result of sensitivity shows that models trained on several datasets (e.g., CIFAR100) can have higher leakage risks than others, which is close to the results of \mathcal{V} -information in general. There are small differences between results of \mathcal{V} -information and sensitivity measure, both in the order of specific datasets (e.g., LeNet on PubFig) and in the specific value of layers’ information leakage risks, which may be due to that attack models cannot capture all changes in the gradients or there are influence factors other than sensitivity.

Latent information. We compute Equation (8) to measure latent information leakage risks. Similar to \mathcal{V} -information, we measure all possible attributes of used datasets and again plot the regression curves for each model. As Figure 5 shows, $\mathcal{R}_l^{(p)}$ generally follows a similar trend as the latent information risks computed using \mathcal{V} -information. That is, the layers related to the classifier have higher leakage risks than the feature extractor layers. Most risks are either in the classifier’s first layer or the second layer. While this is slightly different from the results in Figure 3 where the first layer always has the highest leakage, the overall trend remains the same. We also notice that several scattered points closely coincide, and the last layer has a lower risk compared to that in \mathcal{V} -information. One explanation is that this measure may tend to capture the extreme risks among layers so the first and second layers of the classifier show significantly higher leakage risks than the other layers. Overall, the computation measuring gradient changes (i.e., both sensitivity and subspace distance) depends only on the gradients, is easy-to-compute and captures the main pattern of layer-wise leakage risks measured by attack-based \mathcal{V} -information.

4.3 Hyperparameter impacts

Next, we further explore how the most common training hyperparameters, i.e., aggregation levels and training epochs, affect gradient-based information leakages.

Aggregation levels. Performing aggregation before sharing gradients with others is a very common strategy in federated learning. This could be the *local* aggregation (e.g., batch size in FedSGD or multiple steps in FedAvg) and also the *global* aggregation over updates of all clients. For our aggregation measurement on one target’s (victim) original or latent information, we mix it with

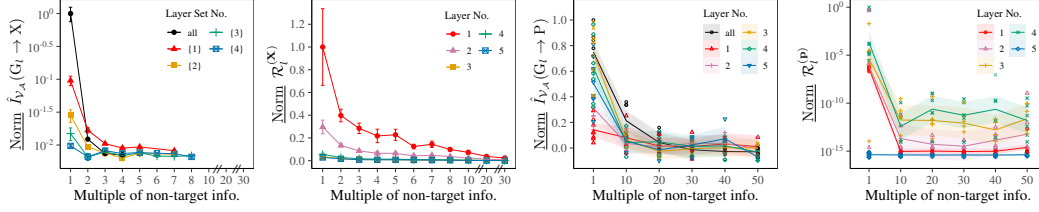


Figure 6: Influence of gradient aggregation on risks of original information [Left two] and latent information [Right two], measured on LeNet trained on CIFAR100 and LFW, respectively (Note: Points corresponding to failed trials of attacks are not plotted. Logarithmic scale is used in some plots for better visualization).

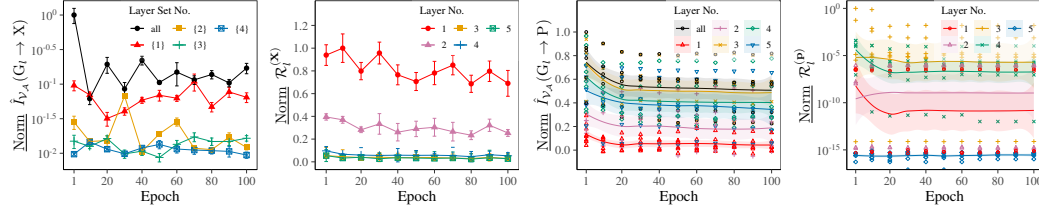


Figure 7: Influence of training epoch on risks of original information [Left two] and latent information [Right two], measured on LeNet trained on CIFAR100 and LFW, respectively.

multiple gradients of non-target information, *i.e.*, information irrelevant to the private information targeted by adversaries. Our empirical results show that aggregation can significantly reduce gradients’ information leakage risks (see Figure 6). Specifically, disclosing target original information from gradients that have been updated on non-target information that is 10 times the amount of target information can be very difficult (*e.g.*, a batch size of 10 in [3, 4]). When gradients are mixed with non-target information that is 30 times the amount of target information, the original information risk measured by sensitivity is extremely low (near zero). Also, extracting latent information from 30~50 times non-target information is hard (*e.g.*, 30~50 participants in [5]).

Epochs. We measure the information leakage risks of gradients at specific epochs (from 1 to 100) during training. As shown in Figure 7, overall the epoch only has a negligible impact on leakage risks. Except for the leakage risk drop in the first several epochs (*i.e.*, first 10 epochs for original information and first 20 epochs for latent information), epochs barely change gradients leakage risks. This may be due to the fact that the magnitude of the updated gradients does not change significantly throughout these epochs (for fixed learning rate). In such a sense, in the first epochs, the ML optimizer quickly converges somewhere near the optimum and increases the model accuracy very quickly; in later epochs, the optimization becomes slower, and consequently, the magnitude of gradient changes stabilizes. This also confirms that gradient changes can be a highly important factor related to private information leakages.

5 Conclusion

Information flow in the backward propagation and related information leakages from gradients are still a conundrum and it cannot be explained by Shannon information. We proposed two mathematically motivated metrics that serve as a major step towards understanding this important open problem. We first adopted \mathcal{V} -information to layer-wisely measure the original and latent information contained in the gradient, and then proposed sensitivity and subspace distance measures to analyze the changes in gradients. Empirical results show that our layer-wise analysis provides a deeper understanding of the memorization of information in neural networks and facilitates the design of flexible layer-level defenses for establishing better trade-offs between privacy and costs.

Limitations. i) A limitation of \mathcal{V} -information-based metrics is the need for specifying the attack family, which we address by proposing metrics that are solely based on changes in the gradients. ii) The choice of normalization, for comparison across layers and models, can affect the interpretation of the leakage risks, leading to challenges in setting thresholds for different leakage risk levels.

Future works. i) It is expected that DNNs with skip connections (*e.g.*, ResNet [57]) could give similar results because they usually have a unidirectional gradient flow, but this needs further experiments. Also, information leakages in other widely used networks such as Recurrent [58] or Graph [59] neural networks need investigating. ii) More defense mechanisms can be analyzed using proposed metrics. For example, the influence of differential privacy can provide a further understanding of the linkage between information leakages and gradient changes (see preliminary results in Appendix A.7). iii) Factors other than sensitivity deserve further exploration. Bayesian-based generalization analysis [60] may help to theoretically characterize information leakages from another perspective.

References

- [1] B. McMahan, E. Moore, D. Ramage, S. Hampson, and B. A. y Arcas, “Communication-efficient learning of deep networks from decentralized data,” in *Artificial Intelligence and Statistics*, 2017, pp. 1273–1282.
- [2] Q. Yang, Y. Liu, T. Chen, and Y. Tong, “Federated machine learning: Concept and applications,” *ACM Transactions on Intelligent Systems and Technology (TIST)*, vol. 10, no. 2, pp. 1–19, 2019.
- [3] L. Zhu, Z. Liu, and S. Han, “Deep leakage from gradients,” in *Advances in Neural Information Processing Systems*, 2019, pp. 14 747–14 756.
- [4] B. Zhao, K. R. Mopuri, and H. Bilen, “iDLG: improved deep leakage from gradients,” *arXiv preprint arXiv:2001.02610*, 2020.
- [5] L. Melis, C. Song, E. De Cristofaro, and V. Shmatikov, “Exploiting unintended feature leakage in collaborative learning,” in *2019 IEEE Symposium on Security and Privacy (SP)*. IEEE, 2019, pp. 691–706.
- [6] M. Nasr, R. Shokri, and A. Houmansadr, “Comprehensive privacy analysis of deep learning: Passive and active white-box inference attacks against centralized and federated learning,” in *2019 IEEE Symposium on Security and Privacy (SP)*. IEEE, 2019, pp. 739–753.
- [7] A. Salem, A. Bhattacharya, M. Backes, M. Fritz, and Y. Zhang, “Updates-leak: Data set inference and reconstruction attacks in online learning,” in *29th {USENIX} Security Symposium*, 2020, pp. 1291–1308.
- [8] J. Geiping, H. Bauermeister, H. Dröge, and M. Moeller, “Inverting gradients—how easy is it to break privacy in federated learning?” *arXiv preprint arXiv:2003.14053*, 2020.
- [9] H. Yin, A. Mallya, A. Vahdat, J. M. Alvarez, J. Kautz, and P. Molchanov, “See through gradients: Image batch recovery via gradInversion,” *arXiv preprint arXiv:2104.07586*, 2021.
- [10] H. Ren, J. Deng, and X. Xie, “GRNN: Generative regression neural network—a data leakage attack for federated learning,” *arXiv preprint arXiv:2105.00529*, 2021.
- [11] S. Yeom, I. Giacomelli, M. Fredrikson, and S. Jha, “Privacy risk in machine learning: Analyzing the connection to overfitting,” in *2018 IEEE 31st Computer Security Foundations Symposium (CSF)*. IEEE, 2018, pp. 268–282.
- [12] K. Leino and M. Fredrikson, “Stolen memories: Leveraging model memorization for calibrated white-box membership inference,” in *29th {USENIX} Security Symposium*, 2020, pp. 1605–1622.
- [13] N. Carlini, C. Liu, Ú. Erlingsson, J. Kos, and D. Song, “The secret sharer: Evaluating and testing unintended memorization in neural networks,” in *28th {USENIX} Security Symposium*, 2019, pp. 267–284.
- [14] A. M. Saxe, Y. Bansal, J. Dapello, M. Advani, A. Kolchinsky, B. D. Tracey, and D. D. Cox, “On the information bottleneck theory of deep learning,” *Journal of Statistical Mechanics: Theory and Experiment*, vol. 2019, no. 12, p. 124020, 2019.
- [15] R. Shwartz-Ziv and N. Tishby, “Opening the black box of deep neural networks via information,” *arXiv preprint arXiv:1703.00810*, 2017.

- [16] N. Tishby, F. C. Pereira, and W. Bialek, “The information bottleneck method,” *arXiv preprint physics/0004057*, 2000.
- [17] Z. Goldfeld, E. Van Den Berg, K. Greenewald, I. Melnyk, N. Nguyen, B. Kingsbury, and Y. Polyanskiy, “Estimating information flow in deep neural networks,” in *International Conference on Machine Learning*, 2019, pp. 2299–2308.
- [18] M. D. Zeiler and R. Fergus, “Visualizing and understanding convolutional networks,” in *European Conference on Computer Vision*. Springer, 2014, pp. 818–833.
- [19] A. Mahendran and A. Vedaldi, “Understanding deep image representations by inverting them,” in *Proceedings of the IEEE Conference on Computer Vision and Pattern Recognition*, 2015, pp. 5188–5196.
- [20] J. Yosinski, J. Clune, A. Nguyen, T. Fuchs, and H. Lipson, “Understanding neural networks through deep visualization,” *arXiv preprint arXiv:1506.06579*, 2015.
- [21] P. Kairouz, H. B. McMahan, B. Avent, A. Bellet, M. Bennis, A. N. Bhagoji, K. Bonawitz, Z. Charles, G. Cormode, R. Cummings *et al.*, “Advances and open problems in federated learning,” *arXiv preprint arXiv:1912.04977*, 2019.
- [22] F. Mo, H. Hamed, K. Katevas, E. Marin, D. Perino, and N. Kourtellis, “PPFL: Privacy-preserving federated learning with trusted execution environments,” in *Proceedings of the 19th International Conference on Mobile Systems, Applications, and Services*, 2021.
- [23] K. Ganju, Q. Wang, W. Yang, C. A. Gunter, and N. Borisov, “Property inference attacks on fully connected neural networks using permutation invariant representations,” in *Proceedings of the 2018 ACM SIGSAC Conference on Computer and Communications Security*, 2018, pp. 619–633.
- [24] L. v. d. Maaten and G. Hinton, “Visualizing data using t-SNE,” *Journal of Machine Learning Research*, vol. 9, no. Nov, pp. 2579–2605, 2008.
- [25] G. Montavon, K.-R. Müller, and M. Braun, “Layer-wise analysis of deep networks with Gaussian kernels,” *Advances in Neural Information Processing Systems*, vol. 23, pp. 1678–1686, 2010.
- [26] A. Choromanska, M. Henaff, M. Mathieu, G. B. Arous, and Y. LeCun, “The loss surfaces of multilayer networks,” in *Artificial Intelligence and Statistics*. PMLR, 2015, pp. 192–204.
- [27] L. Huang, J. Qin, L. Liu, F. Zhu, and L. Shao, “Layer-wise conditioning analysis in exploring the learning dynamics of dnns,” in *European Conference on Computer Vision*. Springer, 2020, pp. 384–401.
- [28] M. I. Belghazi, A. Baratin, S. Rajeshwar, S. Ozair, Y. Bengio, A. Courville, and D. Hjelm, “Mutual information neural estimation,” in *International Conference on Machine Learning*, 2018, pp. 531–540.
- [29] Y. LeCun, L. Bottou, Y. Bengio, and P. Haffner, “Gradient-based learning applied to document recognition,” *Proceedings of the IEEE*, vol. 86, no. 11, pp. 2278–2324, 1998.
- [30] F. Mo, A. S. Shamsabadi, K. Katevas, S. Demetriou, I. Leontiadis, A. Cavallaro, and H. Haddadi, “DarkneTZ: towards model privacy at the edge using trusted execution environments,” in *Proceedings of the 18th International Conference on Mobile Systems, Applications, and Services*, 2020, pp. 161–174.
- [31] A. Sablayrolles, M. Douze, C. Schmid, Y. Ollivier, and H. Jégou, “White-box vs black-box: Bayes optimal strategies for membership inference,” in *International Conference on Machine Learning*, 2019, pp. 5558–5567.
- [32] B. Hitaj, G. Ateniese, and F. Perez-Cruz, “Deep models under the GAN: information leakage from collaborative deep learning,” in *Proceedings of the 2017 ACM SIGSAC Conference on Computer and Communications Security*. ACM, 2017, pp. 603–618.

- [33] Y. Xu, S. Zhao, J. Song, R. Stewart, and S. Ermon, “A theory of usable information under computational constraints,” in *International Conference on Learning Representations (ICLR)*, 2020.
- [34] Z. Wang, A. C. Bovik, H. R. Sheikh, and E. P. Simoncelli, “Image quality assessment: from error visibility to structural similarity,” *IEEE Transactions on Image Processing*, vol. 13, no. 4, pp. 600–612, 2004.
- [35] A. Achille, G. Paolini, and S. Soatto, “Where is the information in a deep neural network?” *arXiv preprint arXiv:1905.12213*, 2019.
- [36] B. Neyshabur, S. Bhojanapalli, D. McAllester, and N. Srebro, “Exploring generalization in deep learning,” in *Advances in Neural Information Processing Systems*, 2017, pp. 5947–5956.
- [37] J. Sokolić, R. Giryes, G. Sapiro, and M. R. Rodrigues, “Robust large margin deep neural networks,” *IEEE Transactions on Signal Processing*, vol. 65, no. 16, pp. 4265–4280, 2017.
- [38] R. Novak, Y. Bahri, D. A. Abolafia, J. Pennington, and J. Sohl-Dickstein, “Sensitivity and generalization in neural networks: an empirical study,” in *International Conference on Learning Representations (ICLR)*, 2018.
- [39] T. Zahavy, B. Kang, A. Sivak, J. Feng, H. Xu, and S. Mannor, “Ensemble robustness and generalization of stochastic deep learning algorithms,” in *International Conference on Learning Representations Workshop*, 2018.
- [40] G. W. Ding, K. Y. C. Lui, X. Jin, L. Wang, and R. Huang, “On the sensitivity of adversarial robustness to input data distributions,” in *International Conference on Learning Representations*, 2018.
- [41] M. Lecuyer, V. Atlidakis, R. Geambasu, D. Hsu, and S. Jana, “Certified robustness to adversarial examples with differential privacy,” in *2019 IEEE Symposium on Security and Privacy (SP)*. IEEE, 2019, pp. 656–672.
- [42] M. Cissé, P. Bojanowski, E. Grave, Y. Dauphin, and N. Usunier, “Parseval networks: Improving robustness to adversarial examples,” in *International Conference on Machine Learning*, 2017.
- [43] Z. Drmac, “On principal angles between subspaces of Euclidean space,” *SIAM Journal on Matrix Analysis and Applications*, vol. 22, no. 1, pp. 173–194, 2000.
- [44] K. Ye and L.-H. Lim, “Schubert varieties and distances between subspaces of different dimensions,” *SIAM Journal on Matrix Analysis and Applications*, vol. 37, no. 3, pp. 1176–1197, 2016.
- [45] A. Björck and G. H. Golub, “Numerical methods for computing angles between linear subspaces,” *Mathematics of Computation*, vol. 27, no. 123, pp. 579–594, 1973.
- [46] A. Krizhevsky, I. Sutskever, and G. E. Hinton, “Imagenet classification with deep convolutional neural networks,” *Advances in Neural Information Processing Systems*, vol. 25, pp. 1097–1105, 2012.
- [47] K. Simonyan and A. Zisserman, “Very deep convolutional networks for large-scale image recognition,” *arXiv preprint arXiv:1409.1556*, 2014.
- [48] Y. Kim, “Convolutional neural networks for sentence classification,” *CoRR*, vol. abs/1408.5882, 2014. [Online]. Available: <http://arxiv.org/abs/1408.5882>
- [49] A. Krizhevsky *et al.*, “Learning multiple layers of features from tiny images,” *Citeseer*, 2009.
- [50] G. B. Huang, M. Mattar, T. Berg, and E. Learned-Miller, “Labeled faces in the wild: A database for studying face recognition in unconstrained environments,” in *Workshop on faces in ‘Real-Life’ Images: detection, alignment, and recognition*, 2008.
- [51] Z. Liu, P. Luo, X. Wang, and X. Tang, “Deep learning face attributes in the wild,” in *Proceedings of International Conference on Computer Vision (ICCV)*, December 2015.

- [52] N. Kumar, A. C. Berg, P. N. Belhumeur, and S. K. Nayar, “Attribute and simile classifiers for face verification,” in *2009 IEEE 12th International Conference on Computer Vision*. IEEE, 2009, pp. 365–372.
- [53] A. Maas, R. E. Daly, P. T. Pham, D. Huang, A. Y. Ng, and C. Potts, “Learning word vectors for sentiment analysis,” in *Proceedings of the 49th annual meeting of the association for computational linguistics: Human language technologies*, 2011, pp. 142–150.
- [54] B. Verhoeven and W. Daelemans, “CLiPS Stylometry Investigation (CSI) corpus: A Dutch corpus for the detection of age, gender, personality, sentiment and deception in text,” in *LREC*, 2014, pp. 3081–3085.
- [55] W. S. Cleveland and S. J. Devlin, “Locally weighted regression: an approach to regression analysis by local fitting,” *Journal of the American Statistical Association*, vol. 83, no. 403, pp. 596–610, 1988.
- [56] A. Wainakh, F. Ventola, T. Müßig, J. Keim, C. G. Cordero, E. Zimmer, T. Grube, K. Kersting, and M. Mühlhäuser, “User label leakage from gradients in federated learning,” *arXiv preprint arXiv:2105.09369*, 2021.
- [57] K. He, X. Zhang, S. Ren, and J. Sun, “Deep residual learning for image recognition,” in *Proceedings of the IEEE Conference on Computer Vision and Pattern Recognition*, 2016, pp. 770–778.
- [58] A. Sherstinsky, “Fundamentals of recurrent neural network (rnn) and long short-term memory (lstm) network,” *Physica D: Nonlinear Phenomena*, vol. 404, p. 132306, 2020.
- [59] Z. Wu, S. Pan, F. Chen, G. Long, C. Zhang, and S. Y. Philip, “A comprehensive survey on graph neural networks,” *IEEE transactions on neural networks and learning systems*, 2020.
- [60] A. G. Wilson and P. Izmailov, “Bayesian deep learning and a probabilistic perspective of generalization,” *Advances in Neural Information Processing Systems*, 2020.
- [61] Y. Aono, T. Hayashi, L. Wang, S. Moriai *et al.*, “Privacy-preserving deep learning via additively homomorphic encryption,” *IEEE Transactions on Information Forensics and Security*, vol. 13, no. 5, pp. 1333–1345, 2017.
- [62] N. Pinto, Z. Stone, T. Zickler, and D. Cox, “Scaling up biologically-inspired computer vision: A case study in unconstrained face recognition on facebook,” in *CVPR 2011 WORKSHOPS*. IEEE, 2011, pp. 35–42.
- [63] R. Shokri and V. Shmatikov, “Privacy-preserving deep learning,” in *Proceedings of the 22nd ACM SIGSAC conference on computer and communications security*, 2015, pp. 1310–1321.
- [64] B. Jayaraman and D. Evans, “Evaluating differentially private machine learning in practice,” in *28th {USENIX} Security Symposium*, 2019, pp. 1895–1912.

A Appendix

A.1 Notations

Table 1 summarises frequently used notations in this paper.

A.2 Gradient Computation

We revisit how gradients are computed as a function of the input to which later shows the root cause for how a gradient \mathbf{G} can reveal input data \mathbf{X} and information about the property \mathbf{p} . Let $\mathbf{X} = [\mathbf{x}_1, \dots, \mathbf{x}_K]$ be one batch of data consisting of K samples from client c ’s training dataset \mathcal{X}^c , and let $\mathbf{Y} = [\mathbf{y}_1, \dots, \mathbf{y}_K]$ be the corresponding ground truth (*e.g.*, labels for a classification task). The complete training dataset of all C clients is denoted by $\mathcal{X} = \{\mathcal{X}^1, \dots, \mathcal{X}^C\}$. For a DNN model

Table 1: Frequently used notations

Symbol	Meaning	Symbol	Meaning
\mathbf{X}	Original input data (<i>det. mat.</i> ^α)	\bar{X}	Original input data (<i>r. var.</i> ^ε)
\mathbf{y}	Input label (<i>det. vec.</i> ^δ)	\bar{Y}	Input label (<i>r. var.</i>)
\mathbf{T}_l	Intermediate representation of layer l^{th} (<i>det. mat.</i>)	\bar{T}_l	Intermediate representation of layer l^{th} (<i>r. var.</i>)
\mathbf{G}_l	Gradients of layer l^{th} (<i>det. mat.</i>)	\bar{G}_l	Gradients of layer l^{th} (<i>r. var.</i>)
\mathbf{p}	Latent attribute of input data (<i>det. vec.</i>)	\bar{P}	Latent attribute of input data (<i>r. var.</i>)
θ_l	Model parameters of layer l^{th} (<i>det. mat.</i>)	x, y, t_l, g_l, p	Instances of X, Y, T_l, G_l, P
$\mathbf{J}_l^{(\mathbf{G})}(\mathbf{X})$	Input-gradient Jacobian of layer l^{th}	$I(X; G)$	Mutual information between X and G
$\mathcal{R}_l^{(\mathbf{X})}$	Original information risk of layer l^{th}	$\mathcal{V}_{\mathcal{A}}$	Predictive family of Adversary \mathcal{A}
$\mathbb{G}_l^{(0)}, \mathbb{G}_l^{(1)}$	Linear subspaces of layer l^{th} 's gradients; (0) or (1): without or with one attribute	$f_{\mathcal{A}}[g_l](x)$	Density measure at x based on g_l
$d_{\text{Gr}}(\mathbb{G}_l^{(0)}, \mathbb{G}_l^{(1)})$	Grassmann distance between subspaces	$\hat{I}_{\mathcal{V}_{\mathcal{A}}}(\mathbb{G}_l \rightarrow X)$	Empirical \mathcal{V} -information from G_l to X
$\mathcal{R}_l^{(\mathbf{p})}$	Latent information risk of layer l^{th}	$f_{\mathcal{A}}[g_l](p)$	Density measure at p based on g_l
		$\hat{I}_{\mathcal{V}_{\mathcal{A}}}(\mathbb{G}_l \rightarrow P)$	Empirical \mathcal{V} -information from G_l to P

^α*det. mat.* refers to ‘deterministic matrix’;

^δ*det. vec.* refers to ‘deterministic vector’;

^ε*r. var.* refers to ‘random variable’.

with L layers, we denote layer l^{th} 's parameters with \mathbf{W}_l and \mathbf{b}_l ; the weights and biases, respectively. In the *forward propagation* from layer 1st to L^{th} , the layer l^{st} computes

$$\mathbf{A}_l = [\mathbf{a}_{l,1}, \dots, \mathbf{a}_{l,K}] = \mathbf{W}_l \mathbf{T}_{l-1} + \mathbf{b}_l \mathbf{1}^\top,$$

where $\mathbf{W}_l \in \mathbb{R}^{N_l \times N_{l-1}}$, $\mathbf{T}_{l-1} = [t_{l-1,1}, \dots, t_{l-1,K}] \in \mathbb{R}^{N_{l-1} \times K}$, $\mathbf{b}_l \in \mathbb{R}^{N_l}$, $\mathbf{1} \in \{1\}^K$. N_l denotes the size (*i.e.*, the number of neurons) of the layer l^{th} , and \mathbf{T}_{l-1} shows the *intermediate representation* that is the output of the (previous) layer $l-1^{\text{th}}$, and $t_{l-1,k}$ corresponds to one sample k 's outputs. Then, the layer l^{th} 's output is $\mathbf{T}_l = [\sigma(\mathbf{a}_{l,1}), \dots, \sigma(\mathbf{a}_{l,K})] \in \mathbb{R}^{N_l \times K}$, denoted as $\sigma(\mathbf{A}_l)$ for simplicity, where $\sigma(\cdot)$ is the chosen activation function. Note that $\mathbf{T}_0 = \mathbf{X}$ and $\mathbf{T}_L = \hat{\mathbf{Y}}$ the prediction on ground truth.

In the *backward propagation*, the loss ℓ between $\hat{\mathbf{Y}}$ and \mathbf{Y} propagates from the layer L^{th} to 1st. For layer l^{th} , the gradient vector \mathbf{G}_l consists of the gradients of the weights and biases $\{\mathbf{G}_l^{(w)}, \mathbf{G}_l^{(b)}\}$, which are computed using chain rule:

$$\mathbf{G}_l^{(w)} = \frac{\partial \ell}{\partial \mathbf{W}_l} = \frac{\partial \ell}{\partial \mathbf{A}_l} \frac{\partial \mathbf{A}_l}{\partial \mathbf{W}_l} = \frac{\partial \ell}{\partial \mathbf{A}_l} \mathbf{T}_{l-1}^\top \quad (9)$$

$$\mathbf{G}_l^{(b)} = \frac{\partial \ell}{\partial \mathbf{b}_l} = \frac{\partial \ell}{\partial \mathbf{A}_l} \frac{\partial \mathbf{A}_l}{\partial \mathbf{b}_l} = \frac{\partial \ell}{\partial \mathbf{A}_l} \mathbf{1} \quad (10)$$

where $\mathbf{G}_l^{(w)} \in \mathbb{R}^{N_l \times N_{l-1}}$ and $\mathbf{G}_l^{(b)} \in \mathbb{R}^{N_l}$ and have the same size with \mathbf{W}_l and biases \mathbf{b}_l respectively.

The set of all layers' $\mathbf{G}^{(w)}$ and $\mathbf{G}^{(b)}$ in Equation (9) and (10) is the minimum unit to update in FL, *i.e.*, corresponding to the FedSGD. $\mathbf{G}^{(w)}$ and $\mathbf{G}^{(b)}$ are also targeted by adversaries to extract private information of \mathbf{X} or its sub-information *e.g.*, \mathbf{p} . In FedAvg, before updating, more batches of data are fed for training, and the gradients of multiple batches are aggregated together element-wisely by

$$\sum_{\mathbf{x}_i \in \mathcal{X}^c} \{\mathbf{G}_l^{(w)}\}_{\mathbf{x}_i}; \quad \sum_{\mathbf{x}_i \in \mathcal{X}^c} \{\mathbf{G}_l^{(b)}\}_{\mathbf{x}_i} \quad (11)$$

General analysis on gradients' privacy risks. Here we directly analyze how \mathbf{G} leaks information of \mathbf{X} or \mathbf{p} based on Equation (9), (10), and (11). Three *indications* for information leakage from DNN parameters (*i.e.*, gradients) are: (1) One can obtain the layer l^{th} 's input (\mathbf{T}_{l-1}) based on this layer's gradient updates. Because the first layer's input (*i.e.*, \mathbf{T}_0) is \mathbf{X} , the original input is highly likely to be leaked, which has also been shown in previous research [61]. (2) Batch-based SGD (*i.e.*, Minibatch) reduces the potential leakage on one specific data sample $\mathbf{x}_i, i \in 1, \dots, K$, because gradients are computed over all samples in one batch (see Equation (9) and (10)). Aggregation, *i.e.*, the summation

of gradients over multiple batches, also reduces the potential leakage (see Equation (11)). (3) The term $\frac{\partial \ell}{\partial \mathbf{A}_l} = \frac{\partial \ell}{\partial \mathbf{T}_l} \odot \sigma'(\mathbf{a}_l) = \mathbf{W}_{l+1}^\top \frac{\partial \ell}{\partial \mathbf{A}_{l+1}} \odot \sigma'(\mathbf{A}_l)$ (note that \odot is the Hadamard product), indicating that the gradient can potentially contain information of \mathbf{A}_l , \mathbf{W}_{l+1} , \mathbf{b}_{l+1} , and parameters of following layers (i.e., $\mathbf{A}_{l+1}, \dots, \mathbf{A}_L$). However, the DPI (from layer 1st to L^{th}) indicates that \mathbf{T}_{l+1} (or \mathbf{a}_{l+1} here) cannot contain more information on \mathbf{X} than \mathbf{T}_l (or \mathbf{a}_l) in *forward propagation* [14–16].

A.3 Theoretical Basis of \mathcal{V} -information

The \mathcal{V} -information is introduced [33] as a new notion of information theory for a practical situation that is under computational constraints. Without putting a constraint on the type of the functions that can be used (the *predictive family*), the \mathcal{V} -information is equivalent to the Shannon mutual information. Assuming some computational constraints for the attacker is a realistic assumption, which is the core of the many practical cryptographic systems. As a consequence, the Data Processing Inequality does not hold anymore in \mathcal{V} -information, which means processing data \mathbf{X} can create some *usable* information. In our setting, we use \mathcal{V} -information to quantify the usable information that is contained in layers of the neural network. Here we briefly summarize the definitions and assumptions underlying the \mathcal{V} -information. For a full review, we refer to [33].

The setting is as follows: a computationally bounded agent (in our applications the adversary), is trying to predict the outcome of a real-valued random variable Y (the true value of the private feature) using another real-valued random variable X as side information (the gradient of the DNN layer). Let \mathcal{X} and \mathcal{Y} denote the sample spaces of X and Y , respectively and let $\mathcal{P}(\mathcal{X})$ and $\mathcal{P}(\mathcal{Y})$ denote the probability measures on \mathcal{X} and \mathcal{Y} , respectively. Furthermore, let $f : \mathcal{X} \times \{\emptyset\} \rightarrow (\mathcal{Y})$. In other words, $f[x]$ ($f[\emptyset]$) is a probability measure on \mathcal{Y} chosen based on the received side information x (or no side information \emptyset). Then, $f[x](y) \in \mathbb{R}$ is the value of the density evaluated at $y \in \mathcal{Y}$.

The first definition we need is that of a predictive family. Specifically, we assume that the set of models that the agent is able to use due to computational constraints, \mathcal{V} , is a predictive family defined as follows:

Definition 1 \mathcal{V} is a predictive family if for any $f \in \mathcal{V}$ and $P \in \text{range}(f)$ there exists an $f' \in \mathcal{V}$ such that for any $x \in \mathcal{X}$, $f'[x] = P$ and $f'[\emptyset] = P$.

The assumption that \mathcal{V} is a predictive family is referred to as optional ignorance and guarantees non-negativity of the \mathcal{V} -information.

The \mathcal{V} -information is then defined as follows:

Definition 2 Let X and Y be two random variables taking values in $\mathcal{X} \times \mathcal{Y}$, and \mathcal{V} is a predictive family. The predictive \mathcal{V} -information from X to Y is defined as,

$$I_{\mathcal{V}}(X \rightarrow Y) = \inf_{f \in \mathcal{V}} \mathbb{E}_{y \sim Y} [-\log f[\emptyset](y)] \\ - \inf_{f \in \mathcal{V}} \mathbb{E}_{x, y \sim X, Y} [-\log f[x](y)].$$

Intuitively, it is the difference between the expected value of the predictive distribution based on side information and the expected value of the predictive distribution based on no additional information. It thus quantifies the value of adding side-information x into the model. To estimate it numerically we can use,

$$\hat{I}_{\mathcal{V}}(X \rightarrow Y; \mathcal{D}) = \inf_{f \in \mathcal{V}} \frac{1}{|\mathcal{D}|} \sum_{y_i \in \mathcal{D}} -\log f[\emptyset](y_i) \\ - \inf_{f \in \mathcal{V}} \frac{1}{|\mathcal{D}|} \sum_{x_i, y_i \in \mathcal{D}} -\log f[x_i](y_i), \quad (12)$$

where f is one function in \mathcal{V} . A neural network can satisfy the definition of a predictive family, done by setting obtain inf, we can use gradient descent approaches such as SGD or Adam to adjust parameters in f (i.e., weights of the DNN model) similar to [33].

A.4 Evaluation Setup

Model. Our LeNet has two Conv layers with 6 and 16 filter, respectively, of 5×5 size (and each has a max-pooling with a size of (2, 2) after). Then it followed by three FC layers with 120, 84, and d_y neurons. d_y is the output size or the number of classes. AlexNet has five Conv layers with 8, 16, 32, 32, and 32 filters. The first is with size 5×5 and the others are with size 3×3 . The second and the fifth have a max-pooling with a size of (2, 2) after, followed by three FC layers same as the LeNet. VGG9 has five Conv layers with 8, 16, 16, 32, 32, and 32 filters of 3×3 size. The third and the sixth have a max-pooling with a size of (2, 2) after. Then it followed by three FC layers with size of 256, 128, and d_y , respectively. All three models use ReLU activation functions for all layers (except the output layer with Softmax). TextClf has two Conv layers followed by two FC layers. Conv layers have 16 filters with size 3 and 8 respectively, and each has a max-pooling with a size of 2 after. FC layers have 50 and d_y neurons respectively.

Datasets. LeNet, AlexNet, and VGG9 models are trained on CIFAR-100 [49] and *three other image datasets* with attributes, including Labeled Faces in the Wild (LFW) [50], Large-scale CelebFaces Attributes (CelebA) [51], and Public Figures Face Database (PubFig) [52]. The last model (*i.e.*, TextClf) is trained on *two text datasets*: IMDB reviews [53] and CSI corpus [54]. LFW contains 13233 face images (cropped as 62×47 RGB). All images are labeled with around 100 attributes such as gender, race, age, hair color, etc. CelebA contains more than 200k face images of celebrities with 40 attribute annotations such as gender, hair color, eyeglasses, etc. We use a subset of the cropped version (*i.e.*, 15000 images) and resize images to 64×64 RGB. We also use a cropped version (100×100 RGB) of PubFig which contains 8300 facial images made up of 100 images for each of 83 persons [62]. All images are marked with 73 attributes (*e.g.*, gender, race, etc). In IMDB reviews [53] dataset, each review is labeled with sentiment and length, and in CSI corpus [54], each corpus review is labeled with sentiment, veracity, length, grade, etc.

Training Setup. We conduct our experiments on a cluster with multiple nodes where each has 4 Intel(R) Xeon(R) E5-2620 CPUs (2.00GHz), one/two NVIDIA RTX 6000 GPU(s) (24GB), and 24GB/48GB DDR4 RAM. Pytorch v1.4.0 is used for DRAs, sensitivity and subspace distance computations, and Theano v1.0 is used to conduct AIAs. Regarding \mathcal{V} -information on the data reconstruction and the attribute inference, attacks can start from the beginning of training process by default. We refer to our codes for more details of gradient change measures and [4, 5] for attack settings.

A.5 Attributes for Measuring Latent Information

For all datasets, we select a subset of attributes considered as private in our evaluation. In the Table 2, for each item of name ‘X_Y_Z’, X refers to the dataset, Y refers to the classification task, and Z refers to the attribute considered as private latent information.

Table 2: Settings of dataset, tasks, and attributes in latent information-related experiments

○ celeba_gender_bald	⊕ csicorpus_length_antwerpen	● lfw_age_blackskin	⊕ lfw_hair_famale
△ celeba_gender_blackhair	⊗ csicorpus_length_deceptive	● lfw_age_famale	× lfw_hair_male
⊕ celeba_gender_hat	⊕ csicorpus_length_truthful	○ lfw_age_male	◇ lfw_smile_asian
× celeba_gender_nohat	⊗ csicorpus_sentiment_short	□ lfw_glasses_asian	▽ lfw_smile_blackskin
◇ celeba_gender_notbald	⊗ csicorpus_veracity_long	◇ lfw_glasses_blackskin	⊗ lfw_smile_famale
▽ celeba_gender_paleskin	■ csicorpus_veracity_short	△ lfw_glasses_famale	* lfw_smile_male
⊗ celeba_hair_famale	● imdb_sentiment_long	▽ lfw_glasses_male	◇ pubfig_gender_asian
* celeba_hair_male	▲ imdb_sentiment_short	○ lfw_hair_asian	⊕ pubfig_gender_blackskin
◇ celeba_hair_paleskin	◆ lfw_age_asian	△ lfw_hair_blackskin	

A.6 p -norm for Computing Sensitivity

When computing sensitivity, we can use measures with different p -norm to reflect the ability of attackers. In the Figure 8, we show 1-norm and ∞ -norm sensitivity. The results generally show

similar patterns with the results of F -norm sensitivity in the Figure 4: First layers have higher original information privacy risks.

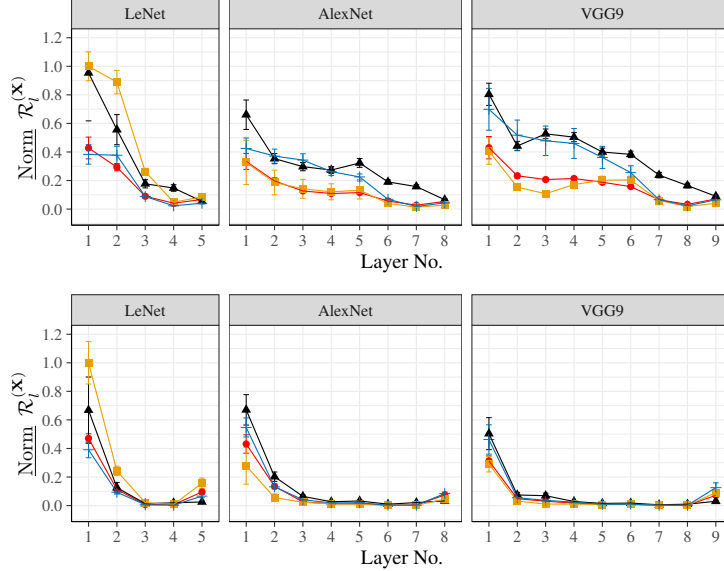


Figure 8: Original information privacy risks, measured by sensitivity ([Top] 1-norm; [Bottom] ∞ -norm), in each layer’s gradients, based on CIFAR100 (—), LFW (—), CelebA (—), PubFig (—) dataset.

A.7 Impact of Differentially Private Training

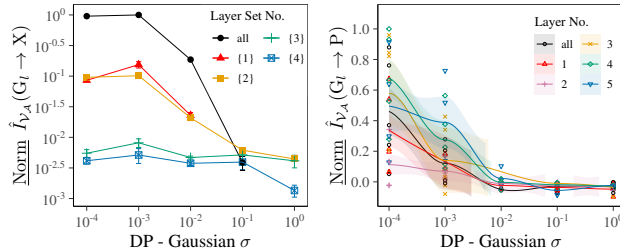


Figure 9: Influence of applying differential privacy on privacy risks of original information [Left] and latent information [Right], measured on LeNet trained on CIFAR100 and LFW, respectively.

Adding differentially private (DP) noises before releasing gradients could be one way to reduce the privacy risks. Here we follow [63, 64], i) to clip gradients using l_2 -norm and then ii) to add Gaussian noises. Specifically, we set the max norm as 1 for all cases and adjust standard deviation σ of Gaussian noises from 10^0 to 10^{-4} . Noises are only added every time before releasing gradients; that is, pre-sample noise addition for data reconstruction attacks, pre-batch (32 samples) noise addition for property inference attacks. We do not tune training hyperparameters or report privacy budget of this DP training for simplicity.

The empirical results are given in Figure 9. According to \mathcal{V} -information measure, DP can reduce the privacy risks of both original and latent information. This is intuitively correct because noises can perturb information in gradients. In addition, we expect that computing privacy risks based on our current gradient change measures may give different answers, *i.e.*, unchanged privacy risks. This explicitly relates to our sensitivity and subspace distance calculations. For sensitivity, adding noises to gradients, *i.e.*, $\mathbf{g}_l(\mathbf{X}) + \mathcal{N}(0, \sigma)$, does not change the derivative results of $\frac{\partial \mathbf{g}_l(\mathbf{X})}{\partial \mathbf{X}}$. For subspace distances, adding noises can spin the subspace, but because i) the subspace has high dimensionality and ii) the magnitude does not influence principal angles, the noises may still do not change the

distances. However, this still follows DP training where the clipping norm decides and controls the sensitivity, which highlights the need of layer-wise clipping for fine-grained privacy risk guarantees.